NUMERICAL METHODOLOGY FOR STUDYING NATURAL CONVECTION ON FLAT AND CORRUGATED PLATES USING OPENFOAM®

Vitor H. T. Santos [a,*], Sílvio. A. Verdério Júnior[b]

Instituto Federal de Educação, Ciência e Tecnologia de São Paulo (IFSP, Department of Industry, CEP 14804-296, Araraquara, SP, Brazil.

[a,*] vitor.taquetto@aluno.ifsp.edu.br, [b]silvioverderio@ifsp.edu.br

ARTICLE INFO

Keywords: *numerical methodology; natural convection; heat transfer; corrugated plate; OpenFOAM®.*

Received: Nov 30, 2024
Reviewed: Dec 08, 2024
Accepted: Dec 15, 2024

ABSTRACT

In recent years, natural convection heat transfer in flat and corrugated plates has been studied, primarily through numerical modeling, to meet the growing demand for more efficient and reliable cooling systems, driven by rapid technological advancements. This work introduces a numerical methodology for investigating heat transfer by natural convection in flat and corrugated plates, utilizing only free and open-source software and tools. The goal is to promote low-cost research and advance the accessibility of scientific studies, by providing a comprehensive technical-scientific guide to literature and enabling replication of the case study. The methodology covers the construction of geometry, mesh generation, case setup, and simulation using OpenFOAM® for a plate with semicircular corrugations. Principal simulation parameters, configuration options, result analysis methods, and potential applications are thoroughly discussed.

NOMENCLATURE

$C_{\varepsilon 1}$	standard empirical constant of $\kappa - \varepsilon$ model
$C_{\varepsilon 2}$	standard empirical constant of $\kappa - \varepsilon$ model
C_{μ}	standard empirical constant of $\kappa - \varepsilon$ model
$\mathbf{g}$	gravity acceleration, m/s²
g_i	indicial gravity acceleration components, m/s²
g_z	z component for gravity acceleration, m/s²
k_t	thermal conductivity, W/(m K)
L_P	plate longitudinal length, m
$\mathbf{n}$	unit surface normal
N	level refinement
Nu	Nusselt number
p	relative total pressure, m²/s²
p_rgh	relative dynamic pseudo-pressure, m²/s²
p_0	relative incompressible total pressure, m²/s²
$\overline{P}$	modified relative turbulent transport pressure, Pa
Pr	Prandtl number
Pr_t	turbulent Prandtl number
q"	convective heat flux over the plate, W/m²
Ra	Rayleigh number
t	time, s
T	temperature, K
T_P	plate temperature, K
T_∞	free-stream temperature, K
$\overline{T}_{REF}$	average reference temperature between $\overline{T}_P$ and $\overline{T}_\infty$, K
u	velocity magnitude, m/s
$\mathbf{u}$	velocity vector, m/s

* Corresponding author: Vitor Santos, Instituto Federal de Educação, Ciência e Tecnologia de São Paulo (IFSP, Department of Industry, CEP 14804-296, Araraquara, SP, Brazil
vitor.taquetto@aluno.ifsp.edu.br

u_i, u_j	indicial velocity components, m/s
U	velocity field OpenFOAM® parameter, m/s
x_i, x_j	indicial coordinates, m
z	elevation. m

Greek symbols

α	thermal diffusivity, m²/s
α_t	turbulent thermal diffusivity, m²/s
β	thermal coeficiente of volume expension, K^{-1}
ε	dissipation rate of turbulent kinetic energy, m²/s³
θ	dimensionless temperature
Δx_0	cell edge at refinement level 0
Δx_N	cell edge at refinement level N
κ	turbulent kinetic energy, m²/s²
μ	dynamic viscosity, kg/(m s)
μ_t	turbulence dynamic viscosity, kg/(m s)
ν	kinematic viscosity, m²/s
ν_t	turbulence kinematic viscosity, m²/s
ρ	fluid density, kg/m³
$\bar{\rho}$	fluid density evaluated in $\overline{T}$, kg/m³
σ_ε	standard empirical constant of $\kappa - \varepsilon$ model
σ_κ	standard empirical constant of $\kappa - \varepsilon$ model
∇	gradient operator

Superscripts

–	average value

1. INTRODUCTION

Convection is a heat transfer phenomenon that occurs in fluids and adjacent surfaces through energy transport mechanisms by diffusion and advection. It can be subdivided into natural, forced and mixed convection. Especially in natural convection, the flow is driven by buoyancy forces that arise due to the temperature gradient in the fluid, which causes density variations. These density differences, combined with the gravitational force, promote the movement of the fluid (Incropera et al., 2008 and Bergman et al. 2014).

The study of natural convection on plates is of great interest in the areas of Engineering due to the simplicity of the geometry, accuracy of the results and great applicability. A notable example is the study of natural convection on corrugated plates to optimize cooling systems, since it operates without the need for external forces (fans, for example), resulting in a reduction in manufacturing and maintenance costs, while also enhancing protection, safety, and reliability (Verdério Júnior et al., 2023).

Although promising, the application is limited to low thermal generation systems, which has spurred further research in the area, seeking new ways to analyze and understand natural convection, mainly through numerical models of flat and corrugated plates. Oosthuizen and Garrett (2001) demonstrate, via numerical simulations that while corrugations in plates alter the flow and reduce heat transfer, the increased surface area they create enhances the overall heat exchange more significantly. Tari and Mehrtash (2013) present $Nu\ x\ Ra$ correlations for natural convection in flat plates with horizontal and inclined fins through numerical studies validated with the experimental literature, varying the gravitational acceleration to analyze the flow and dimensionless results. Hussain et al. (2020) explored natural convection in plates with elliptical and sinusoidal corrugations, analyzing the Nusselt and Rayleigh numbers, the plate aspect ratio and the temperature and fluid flow fields. Muthtamilselvan et al. (2018) numerically study, through the finite volume method, the natural convection of a micropolar fluid in a cavity, heated by orthogonal flat plates, highlighting the behavior of the flow and heat transfer for different Rayleigh values, non-uniformity parameters and vortex viscosities.

Understanding the effects of natural convection in plates enables new studies and applications for optimizing heat exchange processes in various fields. Kousksou et al. (2014) conducted numerical simulations to analyze the Gallium fusion process on wavy surfaces, demonstrating an increase in the fusion rate with increasing wave amplitude. Chen et al. (2019) investigated natural convection heat transfer in two tubes with square flat fins inside a chimney, validating the Nu x Ra correlation and presenting fluid velocity and temperature distributions. In the work presented by Wang and Zhou (2019), numerical simulations were developed to investigate heat transfer by natural convection of liquid metal under the influence of magnetic fields, showing that weaker magnetic fields and smaller Grashof numbers enhance heat transfer.

Specifically in the numerical study of natural convection in corrugated plates the available literature is more limited. Verdério Júnior et al. (2021a) conducted a study to validate and determine the main influential parameters in computational simulations of natural convection in plates, such as boundary conditions, wall functions, mesh refinement, and turbulence models. Verdério Júnior et al. (2021b) presented a methodology and a dimensionless physical-mathematical model for studying natural convection in isothermal plates under turbulent regimes, in addition to discussing the influence of the Grashof, Prandtl, and turbulent Prandtl numbers. Analyses, comparisons, and validations of mesh configurations, physical domain, and boundary conditions were presented by Silva et al. (2021) and Verdério Júnior et al. (2022). Complete studies on heat transfer by natural convection can be found in Verdério Júnior et al. (2023) for flat plates and plates with square, triangular, and trapezoidal corrugations; and in Verdério Júnior (2024) for plates with corrugations of variable height.

Seeking to complement the scientific literature on corrugated plates, this work aims to present a numerical methodology for studying natural convection in flat or corrugated plates. This involves creating the geometry, building and configuring the mesh, determining the parameters, and simulating the case in OpenFOAM®. This methodology can be used for future studies on different and new geometries with applications in various areas of Thermal Engineering. The entire process was conducted using free and open-source software, libraries, and utilities.

2. MATERIALS AND METHODS

2.1 Definition of the Problem Situation

The methodology described in this study is based on the problem situation presented by Verdério Júnior et al. (2023), in which heat transfer by natural convection is evaluated in isothermal flat and corrugated square plates at 40ºC, over a range of Rayleigh numbers. The plate is centered in a large, open physical domain filled with air at an initial temperature of 20ºC.

The modeling and construction of the numerical model representing the phenomenon are carried out by the author, assuming simplifying hypotheses according to Bird et al. (2004) and Versteeg and Malalasekera (2007). The most important ones for this work are briefly presented below.

Air is considered an ideal, Newtonian, incompressible gas with steady-state flow. The variation in density is computed using the Boussinesq approximation to include buoyancy forces, where:

$$\rho(T) \approx \bar{\rho} \cdot [1 - \beta \cdot (T - \overline{T}_{\infty})] \tag{1}$$

Heat exchanges through thermal radiation are considered negligible, given the focus on analyzing heat exchanges through natural convection.

For modeling, the Continuity Equation in turbulent regime is used, as shown in Equation (2); the Momentum Equation in turbulent regime, based on Boussinesq's turbulent viscosity, is presented in Equation (3); and the Energy Equation in turbulent regime is given in Equation (4).

$$\frac{\partial \bar{u}_i}{\partial x_i} = 0 \tag{2}$$

$$\bar{\rho}\left(\frac{\partial \bar{u}_i}{\partial t} + \bar{u}_j \frac{\partial \bar{u}_i}{\partial x_j}\right) = \frac{\partial}{\partial x_j}\left[(\mu + \mu_t)\left(\frac{\partial \bar{u}_i}{\partial x_j} + \frac{\partial \bar{u}_j}{\partial x_i}\right)\right] - \frac{\partial}{\partial x_i}\left(\overline{P} + \frac{2}{3}\bar{\rho}\kappa\right) + \bar{\rho}\left(1 - \beta(T - \overline{T})\right)g_i \tag{3}$$

$$\frac{\partial \bar{\rho}\overline{T}}{\partial t} + \frac{\partial}{\partial x_j}\left(\bar{\rho}\bar{u}_j\overline{T}\right) = \frac{\partial}{\partial x_j}\left[\left(\frac{\mu}{Pr} + \frac{\mu_t}{Pr_t}\right)\left(\frac{\partial \overline{T}}{\partial x_j}\right)\right] \tag{4}$$

The flow is determined to be in a turbulent regime, a hypothesis verified through comparisons and conclusions from the numerical study by Verdério Júnior et al. (2023). Turbulence modeling is performed with the RANS method, using the $\kappa - \varepsilon$ turbulence model, along with wall treatment through scalable wall functions, according to Pope (2012) and Vieser et al. (2002) in Equations (5), (6), and (7).

$$\nu_t = C_\mu \frac{\kappa^2}{\varepsilon} \tag{5}$$

$$\frac{\partial \kappa}{\partial t} + \bar{u}_j \frac{\partial \kappa}{\partial x_j} = \frac{\partial}{\partial x_j}\left[\left(\nu + \frac{\nu_t}{\sigma_\kappa}\right)\frac{\partial \kappa}{\partial x_j}\right] + \nu_t\left(\frac{\partial \bar{u}_i}{\partial x_j} + \frac{\partial \bar{u}_j}{\partial x_i}\right)\frac{\partial \bar{u}_i}{\partial x_j} - \varepsilon \tag{6}$$

$$\frac{\partial \varepsilon}{\partial t} + \bar{u}_j \frac{\partial \varepsilon}{\partial x_j} = \frac{\partial}{\partial x_j}\left[\left(\nu + \frac{\nu_t}{\sigma_\varepsilon}\right)\frac{\partial \varepsilon}{\partial x_j}\right] + C_{\varepsilon 1}\frac{\varepsilon}{\kappa}\nu_t\left(\frac{\partial \bar{u}_i}{\partial x_j} + \frac{\partial \bar{u}_j}{\partial x_i}\right)\frac{\partial \bar{u}_i}{\partial x_j} - C_{\varepsilon 2}\frac{\varepsilon^2}{\kappa} \tag{7}$$

To solve the governing equations, the Finite Volume Method is employed using the free OpenFOAM® software. The process of selecting and adjusting the numerical discretization and interpolation schemes, the solution methods, preconditioners, numerical tolerances, under-relaxation factors and the use of the SIMPLE pressure-velocity coupling algorithm are references from Moukalled et al. (2015), OpenCFD (2019) and better discussed and presented in Verdério Júnior et al. (2021b) and Verdério Júnior et al. (2022).

The physical model, geometry, and mesh configuration used in the presented methodology are detailed, tested, and validated in the following references. Verdério Júnior et al. (2021c) developed an experimental methodology for studying natural convection in flat and corrugated plates using the global capacitance method; the experimental results obtained were used to construct and validate the corresponding numerical-computational model, presented in Verdério Júnior et al. (2023). The characteristics of the computational physical domain and mesh, boundary conditions, and wall functions in this work are based on the tests and conclusions of Verdério Júnior et al. (2022). In addition to the mesh construction parameters, Silva et al. (2021) determined the optimal size of the non-uniform staggered mesh element with regions of greater refinement, in terms of precision and computational cost. The adopted parameters are presented in more detail throughout the work.

Based on the above, the methodology described in this work can be divided into four main stages: construction of the study geometry, mesh generation, structuring/simulation of the case in OpenFOAM®, and analysis of the results. All steps were performed using exclusively free and open-source software, utilities, and

libraries, as summarized in Figure 1, and will be detailed and discussed below.

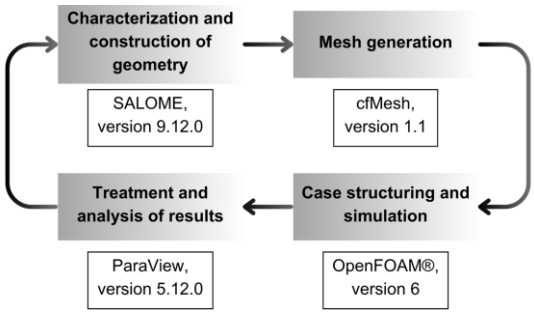

Figure 1. Sequential process of building the numerical model, with main software, libraries and utilities used along with their respective versions.

2.2 Construction of Computational Geometry

The first step is to define the geometry of the study. Based on the conclusions of Verdério Júnior et al. (2023), the importance of the chosen plate geometry is evident, as it can directly impact fluid flow and heat transfer rate – and consequently the effectiveness of the exchange process. To study and construct this methodology, a square plate with equally spaced semicircular corrugations of constant height was considered, as shown in Figure 2. The plate is centered at the bottom of a physical domain where the equations are applied and solved. Its dimensions and shape are also shown in the figure.

In this work, applying the double symmetry condition along the x and y axes is an approach that reduces computational effort and simulation time, simplifying the entire problem to a quarter of its original dimensions. Consequently, the computational models of the geometry were built in the free software SALOME, considering the dimensions defined relative to the dotted symmetry line shown in Figure 2. The models of the physical domain and the plate were built separately in the software. The complete computational model is illustrated in Figure 3.

To apply boundary conditions, the plate and physical domain need to be divided into regions that represent the boundaries of the problem. This division can be performed in SALOME using the *Create Group* tool. For the constructed plate model, the top surfaces, including the corrugations, and side surfaces are defined as a single plate group and exported in STL format. The physical domain is divided similarly, with each surface of the parallelepiped representing a group: front, right, back, left, bottom, and top. Figure 3 illustrates the final model of the problem, with each group identified on its respective surface, and Figure 4 exemplifies the process of separating the plate regions using *Create Group* in SALOME.

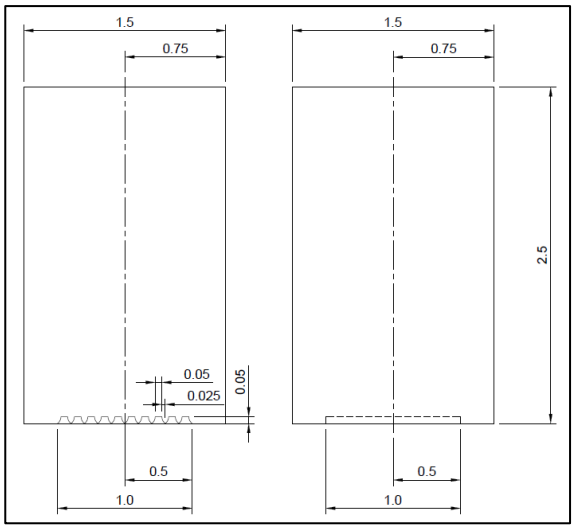

Figure 2. Front and side view of the physical domain and the plate, with dimensions in meters and representation of a quarter by the dotted line of symmetry.

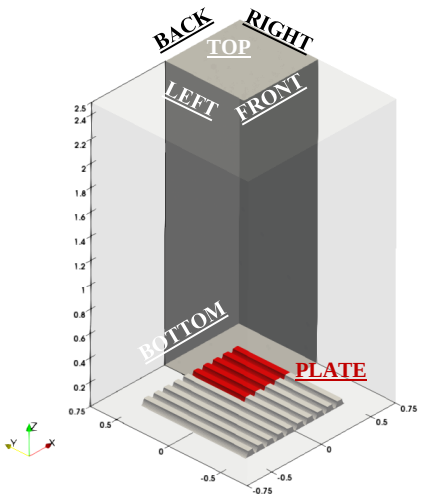

Figure 3. Computational model of the problem, showing the plate and physical domain dimensions in meters, and simulated region (of a quarter) highlighted, with identification of the regions.

To facilitate the identification of these regions during mesh construction, through a text editor, such as Notepad++ version 8.6.7 used in this study, all previously generated files are labeled in the first line immediately after the *solid* parameter with their respective region names. This process is demonstrated in Figure 5 for plate identification.

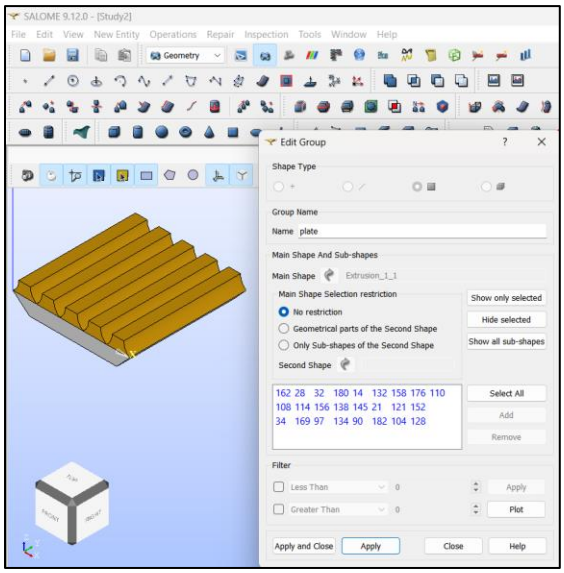

Figure 4. Process of selecting plate surfaces for group creation in the SALOME Create Group tool interface.

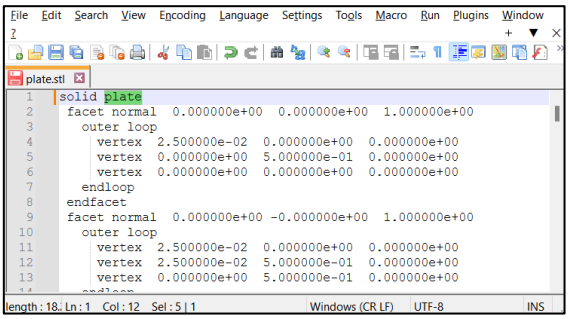

Figure 5. Notepad++ interface for adding the name (highlighted) to the generated file of the plate region.

2.3 Mesh Generation

The mesh representing the physical domain of the problem is constructed using the *cfMesh* utility, implemented in OpenFOAM® software. First, the previously generated STL files must be placed in a mesh directory, which can be obtained from the tutorials provided by the software and follows a basic structure, as shown in Figure 6.

The description of the directories, subdirectories and parameters will be discussed below, exemplifying those used to study this methodology, according to the definitions of Juretic (2015) and the results of Silva et al. (2021) and Verderio Júnior et al. (2022 and 2023).

In general, the mesh file consists of the *constant* and *system* directories. The *constant* directory stores the post-generation mesh files in the *polyMesh* subdirectory – these files define the constructed mesh and are used to simulate the case. The *system* directory contains four subdirectories that define the mesh construction parameters: *controlDict*, *fvSchemes*, *fvSolution*, and *meshDict*. Specifically, *meshDict* allows the configuration of the main generation and refinement parameters of the mesh. Finally, the *mesh* file (FOAM type) enables viewing of the generated mesh in ParaView.

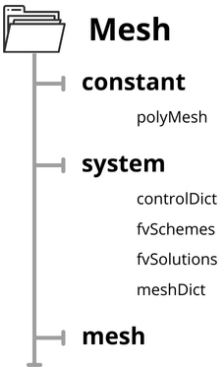

Figure 6. Basic mesh file structure available in cfMesh tutorials.

This study considers the use of a three-dimensional mesh with cartesian hexahedral elements to determine the generation parameters in the *meshDict* subdirectory, of which the following will be described: *maxCellSize*, *surfaceFile*, *objectRefinements*, *additionalRefinementLevels* and *localRefinement*. Their effects can be observed in Figure 7.

The *maxCellSize* parameter defines the default size of the cells generated in the mesh and the maximum size they can have; a value of *maxCellSize* = 0.9 was used. The *surfaceFile* parameter specifies the name and extension of the geometry file that serves as the basis for the mesh, which will be discussed later.

The *objectRefinements* parameter defines the domain refinement zones and their respective geometries. In this study, three regions with varying refinement levels were established, each with a *box* type geometry centered at the origin, with dimensions in x, y, and z as specified in Table 1 and zones demonstrated in Figure 7. Additionally, the *additionalRefinementLevels* keyword, within the *objectRefinements* parameter, specifies the added refinement level in the cells of each zone, in the form of Equation (8). Figure 7 illustrates the effect of the adopted refinement levels.

$$\Delta x_N = \frac{\Delta x_0}{2^N} \tag{8}$$

Table 1. Refinement levels of the zones (box type) defined with objectRefinements and respective dimensions.

Nível do refinamento	Dimensões [m]		
	x	y	z
5	1,000	1,000	2,500
6	0,750	0,750	1,250
7	0,500	0,500	0,625

Finally, the localRefinement parameter enables enhanced refinement in regions of interest in the

physical domain, using the *cellSize* keyword. It defines the edge length of the refined cells in the specified geometry's region/surface, ensuring a uniform and distortion-free mesh – especially useful for complex geometries, with fine details such as edges and curves. For this study, a *cellSize* of 2.5 mm was applied to the plate region, as shown in Figure 7.

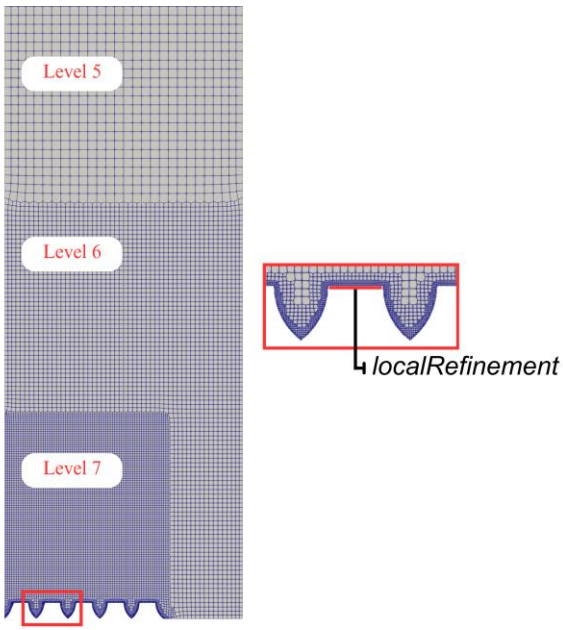

Figure 7. Influence on cell size with application of box type zones with different levels of refinement and with localRefinement in the plate region.

To prepare the mesh generation files, a series of commands must be used in a terminal compatible with the OpenFOAM® version in use. In this work, version 18.04.6 of the Ubuntu LTS platform was adopted. Figure 8 lists the sequential process of commands implemented within the mesh directory. The *cat* command combines all geometry files into a single file called "combined." The *surfaceFeatureEdges* command converts the file format from STL to FMS, which, according to Juretic (2015), can contain all the necessary geometry information for correct mesh generation. The name of this file must match the one specified in the *surfaceFile* parameter of the *meshDict* directory.

Before using the *cartesianMesh* command to generate the mesh, it is necessary to define the conditions of each region of the geometry according to the problem situation, ensuring that this information is incorporated into the mesh. Using a text editor, in the FMS format "combined" file, the regions separated during geometry construction must be identified with the appropriate parameter after each region's name.

The *patch* parameter defines a free surface boundary, allowing energy and matter flow; the *symmetry* parameter indicates symmetry in the regions; and the *wall* parameter defines a solid wall region, which does not allow mass transfer at the boundary. Figure 9 illustrates the distribution of parameters across the domain regions in accordance with the geometry regions and Figure 10 shows this process in the Notepad++ text editor interface.

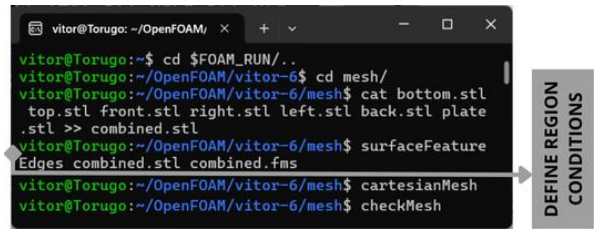

Figure 8. OpenFOAM® terminal interface on Ubuntu, showing the command sequence for preparing files and generating the mesh.

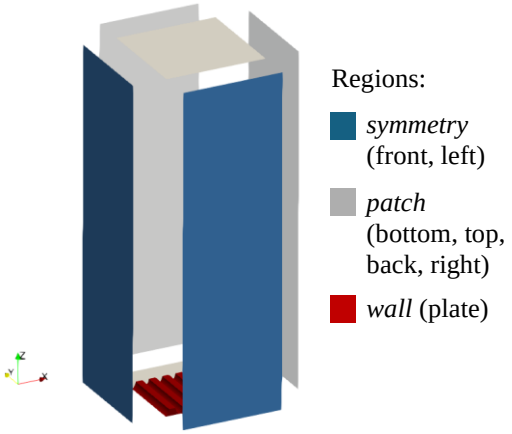

Figure 9. Identification of regions according to surface conditions.

Finally, with the geometry file prepared, the mesh can be generated using the *cartesianMesh* command, as shown in Figure 8. The quality and integrity of the mesh can be checked with the *checkMesh* command, which identifies any potential issues or conflicts in the mesh. Additionally, the free and open-source software ParaView can be used as a complementary tool for visual analysis of the mesh, allowing inspection of possible distortions and inconsistencies, cell structures and refinement regions.

2.4 Case Structuring and Simulation in OpenFOAM®

After constructing and discretizing the geometry, it is necessary to set up the case under study for simulation in OpenFOAM®. This process involves selecting the solver, defining boundary conditions, physical properties and models and other parameters, all within the case directory that, like the mesh directory, can be found in the tutorials provided by the software.

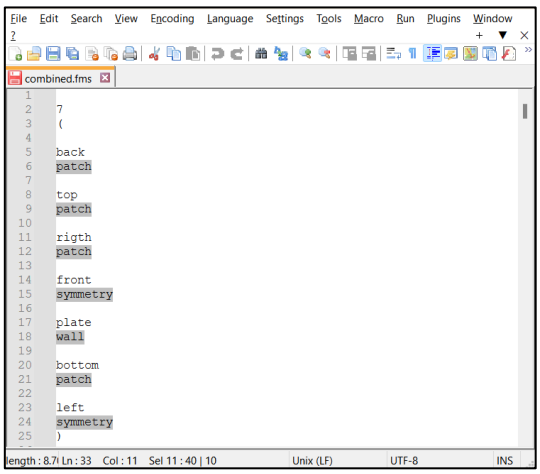

Figure 10. Process of identifying conditions in each region of the mesh geometry in the Notepad++ interface.

The general structure of a case directory, as used in this work, is illustrated in Figure 11, with its components discussed and substantiated according to OpenCFD (2019), Verdério Júnior et al. (2021a), and Verdério Júnior et al. (2023).

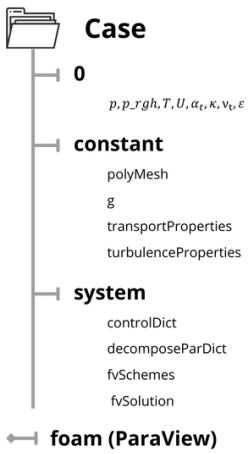

Figure 11. Basic case file structure available in OpenFOAM® tutorials.

The selection of simulation parameters and properties depends on the chosen solver and turbulence model. This study uses the *buoyantBoussinesqSimpleFoam* solver, which accounts for field, weight, and buoyancy forces through the Boussinesq approximation combined with the SIMPLE coupling algorithm. The $\kappa - \varepsilon$ turbulence model is considered in turbulence modeling.

Directory *0* and its subdirectories contain the boundary conditions for the problem. Table 2 associates the parameters defined in each subdirectory with the domain regions for the required properties according to the defined solver and turbulence model. Each parameter in the table is briefly explained and related to its physical equivalent, as referenced in Verdério Júnior et al. (2021a) and OpenCFD (2019).

In the plate region, the following are defined: constant temperature, zero flow velocity, a dynamic pressure gradient for zero velocity, pressure calculation and wall conditions for α_t, κ, ν_t e ε.

In free flow regions, the temperature and velocity gradients are determined based on the flow direction – positive towards the outside of the domain and negative towards the inside. The dynamic pressure is set for incompressible flows, while the other properties are defined as zero-gradient.

In the left and front regions, the symmetry of the problem, as previously discussed, is applied.

Continuing the description of the case directories, in the *constant* directory, the *polyMesh* subdirectory stores the files related to the mesh that will be simulated. This is where the files generated in the mesh directory (*constant*/*polyMesh*) must be allocated.

The g subdirectory defines the components of gravitational acceleration for the problem, according to the orientation of the axes in the constructed geometry. Additionally, since the simulation is performed for a specific range of Rayleigh (Ra) values, a virtual numerical adjustment of gravitational acceleration is used based on the definition of the dimensionless Rayleigh number. Trought the Equation (9), the changes in Ra are linked to adjustments in gravitational acceleration within the g subdirectory.

$$|\mathbf{g}| = \frac{\nu \cdot \alpha \cdot \mathrm{Ra}}{\beta(\mathrm{T_P} - \mathrm{T_\infty})\mathrm{L_p}^3} \qquad (9)$$

This adjustment allows the properties of the problem to remain constant, changing only gravity as a function of Ra. However, using this approach makes only dimensionless analyses valid, such as the Nusselt number and the dimensionless temperature θ, which will be discussed in the results analysis section.

Still within the *constant* directory, the *transportProperties* subdirectory specifies the physical properties of the problem fluid, evaluated at the average reference temperature $\bar{T}_{REF}$. These properties include kinematic viscosity, density, specific heat, thermal expansion coefficient, Prandtl number (laminar and turbulent) and thermal conductivity.

The last subdirectory, *tubulenceProperties*, allows the selection of turbulence models. In this study, the RANS method with the $\kappa - \varepsilon$ turbulence model was used.

Next, in the *system* directory, the *controlDict* subdirectory defines the simulation control parameters. It also specifies the solver, simulation steps, total number of iterations, result recording frequency, and precision level.

In the *decomposeParDict* subdirectory, the division of the numerical domain for parallel processing can be configured based on the available machine setup, optimizing computational cost and reducing simulation time.

The *fvSchemes* subdirectory defines the numerical discretization and interpolation methods used by OpenFOAM® in the simulation. By default, the plate (L_p). Therefore, it does not accurately represent the characteristics of plates with corrugations, such as changes in the heat exchange area.

$$\overline{\mathrm{Nu}} = \frac{\overline{\mathrm{q}}'' \cdot \mathrm{L_p}}{(\mathrm{T_P} - \mathrm{T_\infty}) \cdot \mathrm{k_t}} \tag{10}$$

Table 2. Boundary conditions applied to the subdirectories of directory *0* of the presented case.

Region	$T\ [K]$	$U\ [m/s]$	p_rgh $[m^2/s^2]$	p $[m^2/s^2]$	$\alpha_t\ [m^2/s]$	κ $[m^2/s^2]$	$\nu_t\ [m^2/s]$	$\varepsilon\ [m^2/s^3]$
plate	*fixedValue uniform* $T_p = 313.15\ K$	*noSlip* $u = 0$	*fixedFlux Pressure* Definition of ∇p_rgh to satisfy the condition of $u = 0$	*calculated* $p_{rgh} = p - g \cdot z$	*Alphat JayatillekeWall Function uniform 0* Standard wall function for α_t	*kqRWall Function uniform 1e-05* Simplified zero gradient condition	*nutkWall Function uniform 0* Wall constraint for κ	*Epsilon WallFunction uniform 4e-06* Wall constraint for ε
top	*Inlet Outlet* $\nabla\bar{T} = 0$, if $\boldsymbol{u} \cdot \boldsymbol{n} \geq 0$ $\nabla\bar{T} = \nabla\bar{T}_\infty$, if $\boldsymbol{u} \cdot \boldsymbol{n} < 0$	*pressureInlet Outlet Velocity* $\nabla u = 0$, if $\boldsymbol{u} \cdot \boldsymbol{n} \geq 0$ Calculation of normal components of u from p_rgh, if $\boldsymbol{u} \cdot \boldsymbol{n} < 0$	*total Pressure* $p = p_0 - 0.5^2 \cdot u^2$		*zeroGradient*			
back								
right								
bottom								
left	*symmetry*							
front								

software employs the Finite Volume Method. The *fvSolution* subdirectory specifies the methods for solving the equations, as well as the tolerances, coupling algorithms, and control mechanisms, as best presented in Verdério Júnior et al. (2023).

Finally, the *foam* file represents an executable used to visualize simulation results in ParaView. With this file, temperature distributions, velocities, flow currents, vectors, and various other properties can be viewed in multiple ways and combined with other analysis tools.

With everything described, the case simulation is initiated in the OpenFOAM® terminal, within the case directory, using the command *./Allrun*.

2.5 Analysis of Results

Due to the limitations of the virtual alteration of gravity mentioned above it is valid to analyze, from the simulation results, dimensionless numbers and properties, such as the average Nusselt number and the dimensionless temperature.

The average Nusselt number ($\overline{Nu}$) can be used to compare the efficiency of heat exchange by natural convection in similar cases, such as when there is only variation in Ra. In its common form, represented by Equation (10), only the characteristic length of the problem is considered – in this case, the length of the As verified by Verdério Júnior et al. (2023), the presence of corrugations on the plate creates regions of fluid stagnation that reduce the heat flow in the process. However, the increased heat exchange area due to the corrugations greatly enhances the heat exchanged and the effectiveness of the process. To account for the difference in areas in $\overline{Nu}$, the ratio between the total exchange area and the projected area of the geometry is considered, expressed as $\overline{Nu} \cdot (A/A_p)$. This adjustment ensures that the effects of the increased area are incorporated, while maintaining the dimensionlessness of the number.

The average heat flux by natural convection on the plate, $\bar{q}''$, as given by Equation (10), can be obtained using the *wallHeatFluxIncompressible* utility, compatible with the version of OpenFOAM® in use. This utility calculates the values of heat exchange and total exchange area, recording them in the case directory for each iteration, thereby enabling post-processing and data analysis.

To study and compare temperature fields, or thermal plumes, it is necessary to consider the dimensionless temperature, θ, as shown in Equation (11). This equation can be incorporated into ParaView to generate a new type of dimensionless data based on the simulated temperature. Figures 12 and 13 provide examples of possible data analyses and processing in

ParaView, illustrating the thermal plume and fluid flow lines, respectively.

$$\theta = \frac{T - T_\infty}{T_P - T_\infty} \quad (11)$$

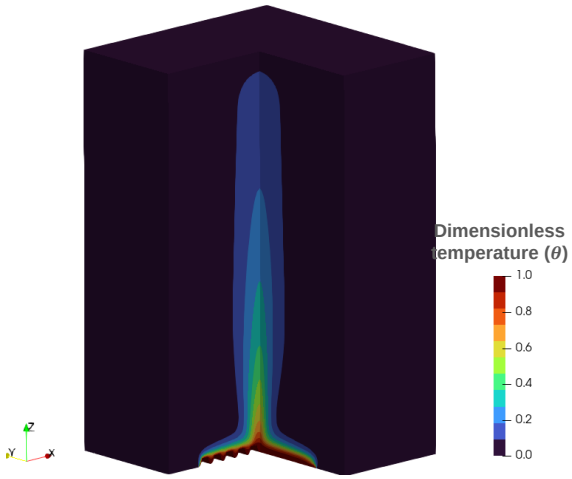

Figure 12. Example of a thermal plume at the center of the physical domain, obtained for **θ** using simulation results and data processing in ParaView.

Figure 13. Fluid flow lines in the plate region obtained with ParaView.

All data processing and analysis involved in developing and presenting this methodology were conducted using a combination of free and open-source software and libraries, such as ParaView for exporting and visualizing results, and Matplotlib and LibreOffice Calc for data comparison and processing.

3. DISCUSSIONS AND CONCLUSIONS

This work demonstrates and discusses a methodology for constructing a numerical study of heat transfer by natural convection on flat and corrugated plates. The case setup involves three main stages: construction of the plate geometry, mesh generation, and structuring/simulation in OpenFOAM®. They are detailed and exemplified for a plate with semicircular corrugations. The entire process utilizes free and open-source software, libraries, and utilities.

The results obtained through this methodology can be used to compare the thermal effectiveness of different geometries in heat transfer by natural convection. The obtainable values for average Nusselt number, analyzed Rayleigh range, thermal plume and flow behavior on the plate for each case serve as a subsidy for further research in the field. These insights also enable optimizations and new technological applications, such as enhancing cooling systems in electronic and microelectronic processing components.

The possibility to change the presented parameters and add new ones enables the simulation to be tailored in various ways, allowing for more specific or broader results and with different levels of precision. Additional physical properties can also be analyzed, different solvers incorporated, and alternative turbulence models or laminar flow regimes evaluated, among other options for configuring the simulation. Furthermore, this methodology can serve as a foundation for new numerical studies, addressing distinct and more complex scenarios, including other heat transfer phenomena, such as radiation, and geometries beyond the plate.

Overall, the methodology presented aims to provide, in the current scientific literature, a technical-scientific manual for studies of natural convection, with the exclusive use of free and open-source software and tools, in order to guarantee accessibility and democratization of science, as a countermeasure to the increasing budgetary restrictions in the field.

4. ACKNOWLEDGEMENTS

The authors thank Instituto Federal de Educação, Ciência e Tecnologia de São Paulo (IFSP), Araraquara campus for providing the resources and support to produce this research project.

5. REFERENCES

Bergman, T. L., Lavine, A. S., Incropera, F. P. and De Witt, D. P., 2014. Fundamentos da Transferência de Calor e de Massa. LTC (in Portuguese).

Bird, R. B., Stewart, W.E. and Lightfoot, E. N., 2004, Transport Phenomena, John Wiley & Sons.

Han-Taw Chen, Wei-Xuan Ma, Pei-Yu Lin, 2019, Natural convection of plate finned tube heat exchangers with two horizontal tubes in a chimney: Experimental and numerical study, International Journal of Heat and Mass Transfer, Vol. 147. DOI: https://doi.org/10.1016/j.ijheatmasstransfer.2019.118948.

Hussain, S., Kalendar, A., Rafique, M. Z., Oosthuizen, P. H., 2020, Assessment of thermal characteristics

of square wavy plates. Heat Transfer, Vol. 49, No. 6, pp. 3742–3757. DOI: https://doi.org/10.1002/htj.21798.

Incropera, F. et al., 2008, Fundamentos da Transferência de Calor e de Massa, LTC (in Portuguese).
Juretic, F., 2015, User Guide cfMesh v1.1.

Creative Fields, Zagreb, Croatia, 2015. URL: http://cfmesh.com/wp-content/uploads/2015/09/User_Guide-cfMesh_v1.1.pdf. Retrieved 28 June 2024.
Kousksou, T., Mahdaoui M. and Ahmed A., 2014,

Numerical Simulation of PCM melting over a wavy surface, International Journal of Numerical Methods for Heat & Fluid Flow, Vol. 24, No. 8, pp. 1660-1678. DOI: https://doi.org/10.1108/HFF-01-2013-0031.

Moukalled, F., Mangani, L. and Darwish, M., 2015, The Finite Volume Method in Computational Fluid Dynamics: An Advanced Introduction with OpenFOAM® and Matlab®, Springer.
Muthtamilselvan M., Periyadurai K. and Doh,

Deog Hee, 2018, Effect of mutually orthogonal heated plates on buoyancy convection flow of micropolar fluid in a cavity, International Journal of Numerical Methods for Heat & Fluid Flow, Vol. 28, No. 9, pp. 2231-2251. DOI: 10.1108/HFF-03-2018-0118.

Oosthuizen, P. H., Garrett, M., 2001, A numerical study of three-dimensional natural convective heat transfer from a plate with a "wavy" surface. ASME International Mechanical Engineering Congress and Exposition, Vol. 35579, American Society of Mechanical Engineers, pp. 119–127.
OPENCFD, 2019, OpenFOAM*:* The Open Source

CFD Toolbox, User Guide (v1906), OpenCFD Ltd.
POPE, S. B., 2012, Turbulent Flows. Cambridge University Press.

Silva, V. R. et al., 2021, Study and Validation of meshes in turbulent isothermal problems of natural convection in flat plates, Revista de Engenharia Térmica, Vol. 20, No. 2, pp. 33-40. DOI: http://dx.doi.org/10.5380/reterm.v20i2.81785.

Tari I. and Mehrtash M., 2013, Natural convection heat transfer from horizontal and slightly inclined plate-fin heat sinks, Applied Thermal Engineering, Vol. 61, No 2, pp. 728-736. DOI: https://doi.org/10.1016/j.applthermaleng.2013.09.003.

Verdério Júnior, S. A. et al., 2021a, Physical–numerical parameters in turbulent simulations of natural convection on three-dimensional square plates, International Journal of Numerical Methods for Heat & Fluid Flow, Vol. 3, No 2, pp. 761–784. DOI: https://doi.org/10.1108/HFF-02-2021-0128.

Verdério Júnior, S. A. et al., 2021b, Dimensionless Physical-Mathematical Modeling of Turbulent Natural Convection, Revista de Engenharia Térmica, Vol. 20, No. 3, pp. 37-43. DOI: http://dx.doi.org/10.5380/reterm.v20i3.83269.

Verdério Júnior, S. A. et al., 2021c, experimental methodology for the study of natural convection on flat and corrugated plates, Revista de Engenharia Térmica, Vol. 20, No. 4, pp. 36-44. DOI: http://dx.doi.org/10.5380/reterm.v20i4.84645.

Verderio Junior, S. A., Scalon, V. L., Del Rio Oliveira, S., Coelho, P. J. M., 2022, Natural convection on corrugated plates: a numerical case study about meshes, boundary conditions and physical domain determination, Revista de Engenharia Térmica, Vol. 21, No. 2, pp. 03–12. DOI: http://dx.doi.org/10.5380/reterm.v21i2.87916.

Verderio Junior, S. A., Coelho, P. J., Scalon, V. L., Del Rio Oliveira, S., 2023, Numerical and experimental study of natural convection heat transfer on flat and corrugated plates, International Journal of Numerical Methods for Heat & Fluid Flow, Vol. 33, No. 9, pp. 3286–3307. DOI: https://doi.org/10.1108/HFF-03-2023-0132.

Verderio Junior, S. A., Coelho, P. J., Scalon, V. L., 2024, Numerical investigation of three-dimensional natural convection heat transfer on corrugated plates of variable height, International Journal of Numerical Methods for Heat & Fluid Flow, Vol. 34, No. 4, pp. 1858-1883. DOI: https://doi.org/10.1108/HFF-10-2023-0591.

Versteeg, H. K. and Malalasekera, W., 2007, An Introduction to Computational Fluid Dynamics – The Finite Volume Method, Longman Scientific and Technical.

Vieser, W., Esch, T., and Menter, F., 2002, Heat transfer predictions using advanced two-equation turbulence models, CFX Validation Report.

Wang Z.H. and Zhou Z.K., 2019, External natural convection heat transfer of liquid metal under the influence of the magnetic field, International Journal of Heat and Mass Transfer, Vol. 134, pp. 175-184. DOI: https://doi.org/10.1016/j.ijheatmasstransfer.2018.12.173.